Journal of Molecular Graphics and Modelling 29 (2011) 876–887

Contents lists available at ScienceDirect

Journal of Molecular Graphics and Modelling

journal homepage: www.elsevier.com/locate/JMGM

Phase-transfer energetics of small-molecule alcohols across the water–hexane interface: Molecular dynamics simulations using charge equilibration models

Brad A. Bauer[a], Yang Zhong[a], David J. Meninger[a,b], Joseph E. Davis[a], Sandeep Patel[a,*]

[a] Department of Chemistry and Biochemistry, 238 Brown Laboratory, University of Delaware, Newark, DE 19716, United States
[b] Department of Physics and Astronomy, University of Delaware, Newark, DE 19716, United States

ARTICLE INFO

Article history:
Received 3 March 2010
Received in revised form
17 September 2010
Accepted 23 September 2010
Available online 1 October 2010

Keywords:
Charge equilibration
Water
Hexane
Interface
Potential of mean force
Alcohols
Methanol
Ethanol
Propanol
Molecular dynamics
Polarizable force fields

ABSTRACT

We study the water–hexane interface using molecular dynamics (MD) and polarizable charge equilibration (CHEQ) force fields. Bulk densities for TIP4P-FQ water and hexane, 1.0086 ± 0.0002 and 0.6378 ± 0.0001 g/cm^3, demonstrate excellent agreement with experiment. Interfacial width and interfacial tension are consistent with previously reported values. The in-plane component of the dielectric permittivity ($\varepsilon_{||}$) for water is shown to decrease from 81.7 ± 0.04 to unity, transitioning longitudinally from bulk water to bulk hexane. $\varepsilon_{||}$ for hexane reaches a maximum in the interface, but this term represents only a small contribution to the total dielectric constant (as expected for a non-polar species). Structurally, net orientations of the molecules arise in the interfacial region such that hexane lies slightly parallel to the interface and water reorients to maximize hydrogen bonding. Interfacial potentials due to contributions of the water and hexane are calculated to be -567.9 ± 0.13 and 198.7 ± 0.01 mV, respectively, giving rise to a total potential in agreement with the range of values reported from previous simulations of similar systems. Potentials of mean force (PMF) calculated for methanol, ethanol, and 1-propanol for the transfer from water to hexane indicate an interfacial free energy minimum, corresponding to the amphiphilic nature of the molecules. The magnitudes of transfer free energies were further characterized from the solvation free energies of alcohols in water and hexane using thermodynamic integration. This analysis shows that solvation free energies for alcohols in hexane are 0.2–0.3 kcal/mol too unfavorable, whereas solvation of alcohols in water is approximately 1 kcal/mol too favorable. For the pure hexane–water interfacial simulations, we observe a monotonic decrease of the water dipole moment to near-vacuum values. This suggests that the electrostatic component of the desolvation free energy is not as severe for polarizable models than for fixed-charge force fields. The implications of such behavior pertain to the modeling of polar and charged solutes in lipidic environments.

1. Introduction

Liquid–liquid interfaces appear in countless physical, chemical, and biological processes. Interfacial mechanisms and dynamics play an important role in industrial applications such as phase-transfer catalysis, electrochemical processes, liquid chromatography, solvent extraction, and interfacial absorption chemistry [1,2]. From a biological perspective, interactions of immiscible liquids at the interface are crucial to membrane processes, interactions at protein receptor sites, the transmission of neural signals, and drug delivery [2,3]. Alcohols, which are used extensively in anesthesiology, and whose toxicity is suggested to be a result of membrane interactions [4–6], are an important class of chemical compounds commonly transported across such interfaces. Moreover, they represent an ideal, prototypical system for studying the energetics of transfer between phases as a proxy for relevant biological systems such as fully hydrated phosphatidylcholine-based bilayers. Despite the prevalence of alcohol-based applications, the fundamental processes governing alcohol transport are not thoroughly understood due to the need for atomic-level resolution that is not easily attainable through experiment [7]. As a result, molecular dynamics (MD) simulation is an important tool for studying such polar–nonpolar interfaces. Indeed, much can be gained from the study of transport energetics across interfaces of polar and nonpolar species since most biological processes involve a polar solvent such as water interacting with nonpolar lipidic systems. From a theoretical standpoint, study of large nonpolar moieties can be simplified through the use of small nonpolar alkanes such as hexane. These water–alkane interfaces have been shown to provide useful models

* Corresponding author.
E-mail address: sapatel@udel.edu (S. Patel).

1093-3263/$ – see front matter © 2010 Elsevier Inc. All rights reserved.
doi:10.1016/j.jmgm.2010.09.005

of the water–membrane interface [8]. To date, the majority of such simulations have utilized traditional fixed charge (nonpolarizable) force fields (see Refs. [8–12] for representative work). However, recent efforts have focused on the development of polarizable force fields, which explicitly model the effects of polarization by allowing for an explicit electrostatic response to changes in local electrostatic fields arising from changes in local chemical environment. Force fields incorporating the effects of polarization include the Drude oscillator [13,14], point-dipole [15,16], and charge equilibration (CHEQ) [17–19] models. Alcohol and hexane force fields have recently been developed within the CHEQ formalism allowing for the study of fully polarizable systems containing these species [20–22]. Certainly, a molecule's ability to modulate its charge distribution in response to its local environment is important when studying the transport energetics across the interface between fluids of vastly different dielectric responses. In addition to their biological relevance, alcohols, due to their amphiphilic nature, provide a more rigorous test of the capabilities of polarizable force fields. Therefore, we investigate the transport energetics of alcohols across the water–hexane interface utilizing polarizable force fields. Such studies are limited in the literature and serve as an important precursor to studies involving transport across solvated membranes. Furthermore, within the context of the current widespread efforts to develop polarizable force fields, the use of charge equilibration force fields for studying such systems will provide a means of comparison to the predictions of current state-of-the-art fixed-charge force fields.

This paper is organized as follows. In Section 2 we discuss the charge equilibration formalism utilized in this work to incorporate polarization into classical simulations, as well as the methods used for simulation. In Section 3 we characterize the thermodynamic and structural properties of the water–hexane interfacial system. The potential of mean force and other properties involved with phase transfer energetics of alcohols in the water–hexane interfacial system are discussed in Section 4. Finally we conclude in Section 5 with a general summary of results.

2. Force fields and computational methods

2.1. Charge equilibration force fields

The charge equilibration (CHEQ) formalism [17–19,23–29] is based on Sanderson's idea of electronegativity equilibration [28,29] in which the chemical potential is equilibrated via the redistribution of charge density. In a classical sense, charge density is reduced to partial charges, Q_i, on each atomic site. The electrostatic energy for a system of M molecules containing N atoms per molecules is then expressed as

$$E_{\text{electrostatic}} = \sum_{k=1}^{M}\sum_{i=1}^{N}\chi_{ik}Q_{ik} + \frac{1}{2}\sum_{l=1}^{M}\sum_{\alpha=1}^{N}\sum_{\beta=1}^{N}\eta_{\alpha l,\beta l}Q_{\alpha l}Q_{\beta l} + \frac{1}{2}\sum_{i=1}^{MN}\sum_{j=1}^{MN}\frac{Q_iQ_j}{r_{ij}} \quad (1)$$

where the χ's are the atom electronegativities which control the directionality of electron flow and the η's are the atomic hardnesses which control the resistance to electron flow to or from an atom. Although these parameters derive from the definitions of electron affinity and ionization potential, they are treated as empirical parameters for individual atom types. Heterogeneous hardness elements that describe the interaction between two different atom types are calculated using the combining rule [30] on the parameterized homogeneous hardness elements:

$$\eta_{ij}(R_{ij},\eta_i,\eta_j) = \frac{(1/2)(\eta_i+\eta_j)}{\sqrt{1.0+(1/4)(\eta_i+\eta_j)^2R_{ij}^2}} \quad (2)$$

where R_{ij} is the distance between atoms i and j. This combination locally screens Coulombic interactions, but provides the correct limiting behavior for atomic separations greater than approximately 2.5 Å. The standard Coulomb interaction between sites not involved in dihedral, angle, or bonded interactions with each other is included as the last term in Eq. (1). The second term in Eq. (1) represents the local charge transfer interaction, which is usually restricted to within a molecule or an appropriate charge normalization unit, i.e., no intermolecular charge transfer. Charge is constrained via a Lagrange multiplier, λ, which is included for each molecule, resulting in the electrostatic energy expression:

$$E_{\text{electrostatic}} = \sum_{k=1}^{M}\sum_{i=1}^{N}\chi_{ik}Q_{ik} + \frac{1}{2}\sum_{l=1}^{M}\sum_{\alpha=1}^{N}\sum_{\beta=1}^{N}\eta_{\alpha l,\beta l}Q_{\alpha l}Q_{\beta l} + \frac{1}{2}\sum_{i=1}^{MN}\sum_{j=1}^{MN}\frac{Q_iQ_j}{r_{ij}} + \sum_{j=1}^{M}\lambda_j\left(\sum_{i=1}^{N}Q_{ji} - Q_j^{\text{Total}}\right) \quad (3)$$

We remark that use of multiple charge normalization units can modulate molecular polarizability by limiting intramolecular charge transfer to physically realistic distances. Such an approach controls previously observed superlinear polarizability scaling [20,31,32], which also manifests as the polarization catastrophe (as observed in point polarizable force fields) [16,32], while developing a construct for piecing together small molecular entities into macromolecules. The molecular polarizability within this formalism can be derived as

$$\alpha_{\gamma\beta} = \mathbf{R}_\beta^t\eta'^{-1}\mathbf{R}_\gamma \quad (4)$$

where η' denotes the molecular hardness matrix *augmented* to incorporate total charge constraints for each charge normalization unit [32]. $\mathbf{R}_\beta$ and $\mathbf{R}_\gamma$ represent the β and γ Cartesian coordinates of the atomic position vectors, respectively.

Charge degrees of freedom are propagated via an extended Lagrangian formulation imposing a molecular charge neutrality constraint, thus providing for electronegativity equilibration at each dynamics step. The system Lagrangian is:

$$L = \sum_{i=1}^{M}\sum_{\alpha=1}^{N}\frac{1}{2}m_{i\alpha}\left(\frac{dr_{i\alpha}}{dt}\right)^2 + \sum_{i=1}^{M}\sum_{\alpha=1}^{N_i}\frac{1}{2}m_{Q,i\alpha}\left(\frac{dQ_{i\alpha}}{dt}\right)^2 - E(Q,r) - \sum_{i=1}^{M}\lambda_i\sum_{\alpha=1}^{N_i}Q_{i\alpha} \quad (5)$$

where the first two terms represent the nuclear and charge kinetic energies, the third term is a potential energy, and the fourth term is the molecular charge neutrality constraint enforced on each molecule i via a Lagrange multiplier λ_i. The fictitious charge dynamics are determined using a charge "mass" with units of (energy time^2/charge^2). This is analogous to the use of an adiabaticity parameter in fictitious wavefunction dynamics in Car Parinello (CP) type methods [33]. Charges are propagated based on the forces arising from differences between the average electronegativity of a molecule and the instantaneous electronegativity at an atomic site.

Finally, nonbonded interactions are treated using a Lennard–Jones type potential:

$$E(r_{ij}) = \sum_{ij} \varepsilon_{ij} \left(\frac{R_{\min,ij}^{12}}{r_{ij}^{12}} - 2\frac{R_{\min,ij}^{6}}{r_{ij}^{6}} \right) \quad (6)$$

in which the summation is over all nonbonded atom pairs. The parameters ε and $R_{\min}$ correspond to the energy well depth and position of minimum potential, respectively. The nonbonded and electrostatic parameters for hexane are taken from Davis et al. [20], parameters for alcohol are taken from Patel and Brooks [21,22], and water (TIP4P-FQ) from Rick et al. [19]. Hexane–water cross interaction parameters are determined using often-used Lorentz–Berthelot (LB) combining rules. We acknowledge that the use of the LB combining rule is an approximation that has come under scrutiny in the recent literature [34–37]. There is no *a priori* reason to implement this particular combining rule (with ample evidence in the literature suggesting that it does not provide the most accurate description of cross-interactions), or off-diagonal non-bond dispersion interactions in the case of noble gas mixtures [34] and polar compounds in the context of hydration free energies [36]; however, for the present study, we apply this combining rule as it is a common practice, and within the context of this approximation, we consider the properties of the heterogeneous systems defined here, acknowledging that the combining rule is a potential source of error between computed properties and experiment. It would prove an interesting and valuable study to compare various combining rule schemes in the context of a broad range of mixture properties of heterogeneous (multi-component) molecular systems, much in the spirit of the literature on noble gases and their mixtures [34,35].

2.2. Simulation protocol

Simulations were conducted in the constant volume and temperature ensemble using the Chemistry at HARvard Molecular Mechanics (CHARMM) package [38]. SHAKE [39] constraints were applied in order to maintain a rigid water geometry. Temperature was maintained at 298 K via a Nosé-Hoover [40,41] thermostat with a thermal inertia parameter of 3000.0 (kcal/mol)/(ps^2). A Verlet leapfrog integrator scheme with a time step of 0.5 fs was used to generate trajectories. An atom-based cutoff distance of 11 Å was utilized for nonbonded interactions. The Smooth Particle Mesh Ewald method [42] was applied to account for long-range electrostatic interactions. A 48 Å × 48 Å × 80 Å FFT grid and a value of $\kappa = 0.33$ for the Ewald dispersion parameter were used. In order to allow for the movement of partial charges within the polarizable model, fictitious masses of 0.0008 ((kcal/mol)ps^2)/e^2 were assigned to all atoms in the hexane molecules; masses of 0.00005 ((kcal/mol)ps^2)/e^2 were assigned to all sites in the water molecules. Fictitious charge masses of 0.000075, 0.000080, 0.000075, and 0.000085 ((kcal/mol)ps^2)/e^2 were assigned to all atoms in the methanol, ethanol, 1-propanol, 1-butanol molecules, respectively. A Nosé-Hoover bath with a thermal inertia parameter of 0.005 (kcal/mol)/(ps^2) was also applied in order to maintain an electronic temperature of 1 K. A separate bath was coupled to each type of molecule within the system. In order to prevent unrealistic intramolecular charge transfer in the larger chain alcohols, 1-propanol and 1-butanol were each divided into two charge normalization units; 1-propanol was partitioned into methyl-like and ethanol-like normalization groups, and 1-butanol was partitioned into ethyl-like and ethanol-like normalization groups. A 42 Å × 42 Å × 81 Å system of 430 hexane and 1535 water molecules was equilibrated to obtain a starting structure. The equilibrated system consisted of a central water layer (spanning a length of ~26 Å) and two hexane layers on each end (each was approximately 27.5 Å long). For the alcohol simulations a single molecule was added to the equilibrated water–hexane system. Results of longitudinally varying properties (i.e., density, potential of mean force, etc.) are presented in symmetrized form with the center of the water layer taken to be the origin.

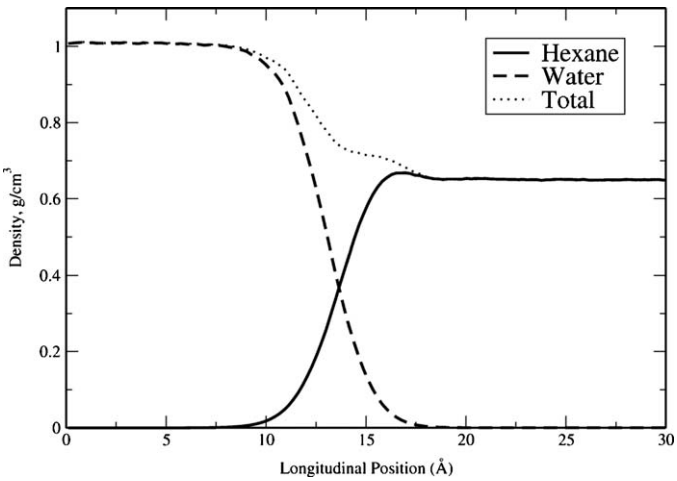

Fig. 1. Density profiles for the water–hexane system. $z = 0$ is the center of mass of the system.

Umbrella sampling was used to calculate potentials of mean force (PMF) for water, hexane, methanol, ethanol and 1-propanol. A harmonic restraint ranging from 1 to 2 (kcal/mol)/Å^2 was applied to the distance in the z-direction between the system's center of mass and the subject molecule. A 1 Å distance was applied between each biasing potential, giving a total of 25 windows for each type of molecule. Each window was run for a minimum of 3 ns yielding more than 75 ns of total simulation for each molecule. PMFs for the molecules were then calculated using the weighted histogram analysis method (WHAM) [43]. Uncertainties were calculated as the standard deviation of the PMF's calculated over separate 1 ns segments of the simulations at each window. Alternatively, thermodynamic integration (TI) was performed to determine the solvation free energies of alcohols in each hexane and water solvent. For the alcohols in hexane, 1 alcohol solute was placed in a periodically replicated, cubic box containing 216 hexane molecules. Interactions between solute and solvent were decoupled in two thermodynamic paths (electrostatic and nonbond), each divided into 21 linearly spaced windows. Five independent simulations with 200 ps of sampling per window (after an initial equilibration period) were performed. Uncertainties are reported as the standard deviation over all independent simulations for each Lennard–Jones and electrostatic decoupling window, with the total hydration free energy uncertainty computed as $\sigma^2 = \sqrt{\sigma_{\mathrm{LJ}}^2 + \sigma_{\mathrm{elec}}^2}$. Hydration free energies of alcohols in water were taken from the work of Zhong and Patel [37].

3. Hexane–water interfacial system

3.1. Thermodynamic properties

3.1.1. Density profiles

We show the density profiles of the hexane-water interfacial system in Fig. 1. Profiles were computed by calculating the mass of all atoms within a slab of a given volume, averaged over all trajectories. Compared to previous molecular dynamics studies of the hexane–water interface employing CHEQ models [44], we see a slight densification of the water phase and rarefaction of the hexane phase. Bulk phase densities were calculated by averaging the

density of each phase over a region far from the interface yielding values of 1.0086 ± 0.0002 and 0.6378 ± 0.0001 g/cm^3 for water and hexane, respectively. The water density is above the experimental and TIP4P-FQ densities [26] while the hexane is below the experimental density (0.6606 g/cm^3) [45]. We note the slight increase in the density of hexane near the interface, which has been observed in simulations of other water–hydrocarbon interfaces [46]. The enhanced hexane density at the interface will be discussed in the context of interfacial structuring of hexane.

The density profiles were used to estimate the total interfacial width, w, which can be computed from the intrinsic width, w_0, and the width due to thermal fluctuations, w_c, as

$$w^2 = w_0^2 + w_c^2 \tag{7}$$

The intrinsic width can be computed from the separation of the Gibbs dividing surfaces as

$$w_0 = \left| \left\langle h_W \right\rangle - \left\langle h_H \right\rangle \right| \tag{8}$$

where $\langle h_W \rangle$ and $\langle h_H \rangle$ are the average location of the Gibbs dividing surface for water and hexane, respectively. To find the Gibbs dividing surface of the water we followed the approach of Senapati and Berkowitz [47] by fitting the individual water density profile to an error function as

$$\rho_W(z) = \frac{1}{2}\rho_{W,\text{bulk}} - \frac{1}{2}\rho_{W,\text{bulk}} \text{erf}\left(\frac{z - \left\langle h_W \right\rangle}{\sqrt{2} w_c} \right) \tag{9}$$

The hexane density profile could not be sufficiently fit to an error function due to the slight densification of the hexane near the interface. To account for this a Gaussian function was included to minimize the effect of this peak on the error function fit as

$$\rho_H(z) = \rho_{H,\text{bulk}} + \rho_{H,\text{bulk}} \text{erf}\left(\frac{z - a}{w_c} \right) + b \exp\left(\frac{-(z-c)^2}{d} \right) \tag{10}$$

where a, b, c and d are parameters empirically fit to the data. The Gibbs dividing surface for the individual hexane profile, $\langle h_H \rangle$, was then found by solving for the location at which the surface excess equals zero. Surface excess is defined as [29,48,49]

$$\Gamma = \int_0^{\langle h_H \rangle} dz \left[\rho_H(z) \right] + \int_{\langle h_H \rangle}^{\infty} dz \left[\rho_H(z) - \rho_{H,\text{bulk}} \right]. \tag{11}$$

We predict a thermal contribution of 1.795 ± 0.004 Å and an intrinsic width contribution of 0.13 ± 0.04 Å. w_0 is lower than expected but can be explained by the densification of hexane at 15.5 Å, which causes the Gibbs dividing surface to shift closer towards the bulk water. This yields a total interfacial width of 1.80 ± 0.04 Å with the majority of the thickness being due to the thermal contributions.

3.1.2. Interfacial tension

The water–hexane interfacial tension is computed from the components of the internal pressure tensor as the difference between the normal and tangential pressures [50–52]:

$$\gamma = \frac{L_z}{2} \left[\left\langle P_{zz} \right\rangle - \frac{1}{2} \left(\left\langle P_{yy} \right\rangle + \left\langle P_{xx} \right\rangle \right) \right] \tag{12}$$

where the pressure tensor components, $P_{\alpha\alpha}$, are computed from the standard definition of the atomic virial [40] and L_z is the z-dimension of the simulation box. The water–hexane interfacial tension at 298 K was computed to be 43.9 ± 0.8 dyn/cm. This value is below the experimental value of 50.0 dyn/cm [10,53] but shows improvement from earlier CHEQ parameterizations and the nonpolarizable C27r model, which yielded interfacial tensions of 43.24 ± 0.4 and 42.27 ± 0.25 dyn/cm, respectively [44]. Furthermore, ongoing improvements to the hexane–water interaction potential via refinement of hydration free energies will afford better agreement of the computed surface tension to experiment; the current model overestimates the water–hexane interaction based on the hexane hydration free energy of 1.80 ± 0.5 kcal/mol [20]. Nevertheless, the force field is of sufficient quality to consider the behavior of solute properties across the polar–nonpolar interface.

3.1.3. Dielectric permittivity profiles

Since the transfer from polar to non-polar medium is intimately related to a change in the dielectric response of the surrounding medium (vis-à-vis Clausius–Mossotti relation), we next consider the variation in dielectric constant transitioning through the water phase to the hexane phase. The nature of the dielectric constant and its variation has been implicated in the preferential partitioning of polarizable ions at the aqueous liquid–vapor interface of inorganic salt solutions [54]. Moreover, there is evidence from molecular dynamics simulations of methanol–water interfaces repelling inorganic anions [55]. We use an approach developed by Stern and Feller [56] for computing the longitudinal profile for the parallel (in-plane) component of the dielectric constant. The parallel component of the dielectric permittivity is calculated as a function of z, the dimension in which the system is non-uniform, using Eqs. (71) and (26) of Stern and Feller [56]:

$$\varepsilon_{||} = (4\pi\, h_{||}(z)) + 1 \tag{13}$$

$$h_{||}(z) = \frac{1}{2k_B T} \left\langle \mathbf{P}_{||}(z) \cdot \mathbf{M}_{||} \right\rangle + \left\langle a_{||}(z) \right\rangle \tag{14}$$

where $\mathbf{P}_{||}(z)$ is the local polarization density and $\mathbf{M}_{||}$ is the *total* system dipole moment. The present approach self-consistently includes polarization contribution, $\alpha_{||}(z)$, in the first term of Eq. (14). The polarization density is computed using a bond-charge approach outlined by Stern and Feller and briefly discussed here. The charge on a particular atom, i, is determined using a set of bond-charge increments (bci's), denoted b_{ij}. Each atom associated with a particular bci, b_{ij}, will receive an amount of charge $\pm b_{ij}$. The total charge on an atom is then taken as the sum over all contributions from bci's including that atom as represented in the mapping:

$$q_i = \sum_{jk} C_{i,jk} b_{jk} \tag{15}$$

with

$$C_{i,jk} = \begin{cases} 1 & i = j \\ -1 & i = k \\ 0 & i \neq k;\ i \neq j \end{cases}. \tag{16}$$

From a given set of charges, the bci's are obtained via inversion of the C matrix using singular value decomposition [56] or straightforward inversion (for well-conditioned matrices). The inverse is calculated once for a given molecule and is reused for analysis of the simulation trajectory. The polarization density is then calculated from the sum of local bond charge dipole moments at a position z:

$$\mathbf{P}(z) = \frac{1}{A} \sum_{jk} \mu_{jk} \delta(z - z_{jk}) \tag{17}$$

where the bond dipole is simply

$$\mu_{jk} = b_{jk}(r_j - r_k). \tag{18}$$

Fig. 2A and B give the profiles of the in-plane component, $\varepsilon_{||}$, for water and hexane. The bulk values of $\varepsilon_{||}$ for water and hexane are 81.7 ± 0.4 and 1.0054 ± 0.0004. Both profiles exhibit a slight increase at the interface with the dielectric of water increasing to 91.9 and the dielectric of hexane increasing to 1.097. The total

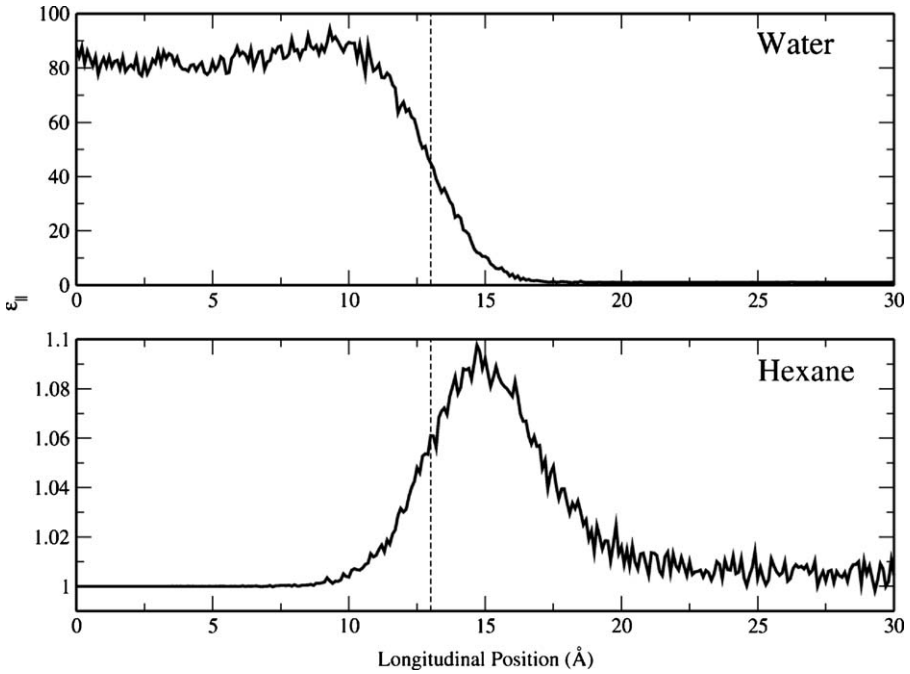

Fig. 2. In-plane dielectric permittivity, $\varepsilon_{||}$, of water and hexane as a function of longitudinal position relative to the center of mass of the system. The total system Gibbs dividing surface is indicated by the dashed vertical line.

dielectric permittivity can be approximated using the parallel component $\varepsilon_{||}$ and the dielectric constant at infinite frequency ε_∞ as

$$\varepsilon = \varepsilon_{||} + \varepsilon_\infty - 1. \tag{19}$$

Rick et al. [19] report an ε_∞ of 1.592 for TIP4P-FQ. Adding $\varepsilon_{||}$ to ε_∞ yields an ε of 83.3 which is ~7% above the experimental value of 78 [45]. For hexane, ε_∞ was estimated by the Clausius–Mossotti equation:

$$\frac{\varepsilon_\infty - 1}{\varepsilon_\infty + 2} = \frac{4\pi}{3}\frac{\alpha}{\langle V \rangle} \tag{20}$$

where α represents the molecular polarizability and $\langle V \rangle$ is the average molecular volume. Using values calculated for the molecule ($\alpha = 11.735$ Å^3 [20] and $\langle V \rangle = 224.5$ Å^3, respectively), and ε_∞ is computed to be 1.84. The contribution of $\varepsilon_{||}$ is negligible (arising from the low-frequency modes characteristic of nuclear motion that are more important in defining the dielectric response of strongly polar molecular species), resulting in a total ε of 1.84 for hexane, which is slightly below the experimental value of 1.88 [45]. We note that using the model polarizability and the molecular volume from the experimental density of 0.6606 g/cm^3, the correct dielectric permittivity is obtained, indicating that the discrepancy is due to the density, not the polarizability.

3.2. Structural properties

3.2.1. Interfacial structure

It has been observed that long chain molecules, ranging in size from decane to eicosane, exhibit a net preferential chain formation at an interfacial region [50,57], the interface being either between the bulk fluid alkane and its vapor or the interface between water and an alkane. This interfacial orientational ordering is in contrast with the random conformational behavior associated with molecules in a bulk isotropic environment. We consider the effect of the interface on the orientation of molecules by defining the order parameter [50,57]:

$$S_{ZZ} = \frac{1}{2}\left\langle (3\cos^2(\theta) - 1) \right\rangle. \tag{21}$$

For hexane the angle θ is defined as the angle between the normal of the interface and the vector from carbon n to carbon $n+2$, resulting in four C_n–C_{n+2} vectors per hexane molecule; this angle defines a local orientational of the angle. The average was taken over all vectors in all hexane molecules within a given region in order to generate a z-dependent profile. A value of 1 signifies an average orientation of all vectors perpendicular to the interface while a value of −0.5 denotes an average orientation parallel to the interface. A value of $S_{ZZ} = 0$ indicates completely random orientation. For water we report average orientation as the cosine of the angle, θ, between the normal of the interface and the permanent dipole; this is referred to as $\langle \cos\theta \rangle$ which takes values of ±1 when permanent dipoles are aligned with the positive/negative z-axis (interface normal) and values of 0 for isotropic orientations. Fig. 3 shows the hexane and water orientation profiles. As is anticipated from a bulk isotropic environment, bulk hexane and water display a random orientation. As they enter the interface ($z = 7$), the water molecules align such that the hydrogen atoms point towards the bulk water. This orientation allows for the maximum occurrence of hydrogen bonding. However, when entering the bulk hexane ($z = 14$), the orientation of water is reversed and the hydrogen atoms point towards the bulk hexane. Interestingly, this behavior is similar, albeit not as pronounced, to TIP4P-FQ water at the liquid–vapor interface [58]. Once fully submerged in the bulk hexane, water again assumes a random orientation. Moving towards the interface from the bulk hexane phase, hexane molecules preferentially orient parallel to the interface beginning near the region $z = 18$ and continuing towards the water phase. This behavior is similar to that exhibited by several decane models studied in the context of the decane–water interface [57]. However, hexane in the present study is not as severely aligned perpendicular to the interface normal as is decane in Ref. [57]. Moving further

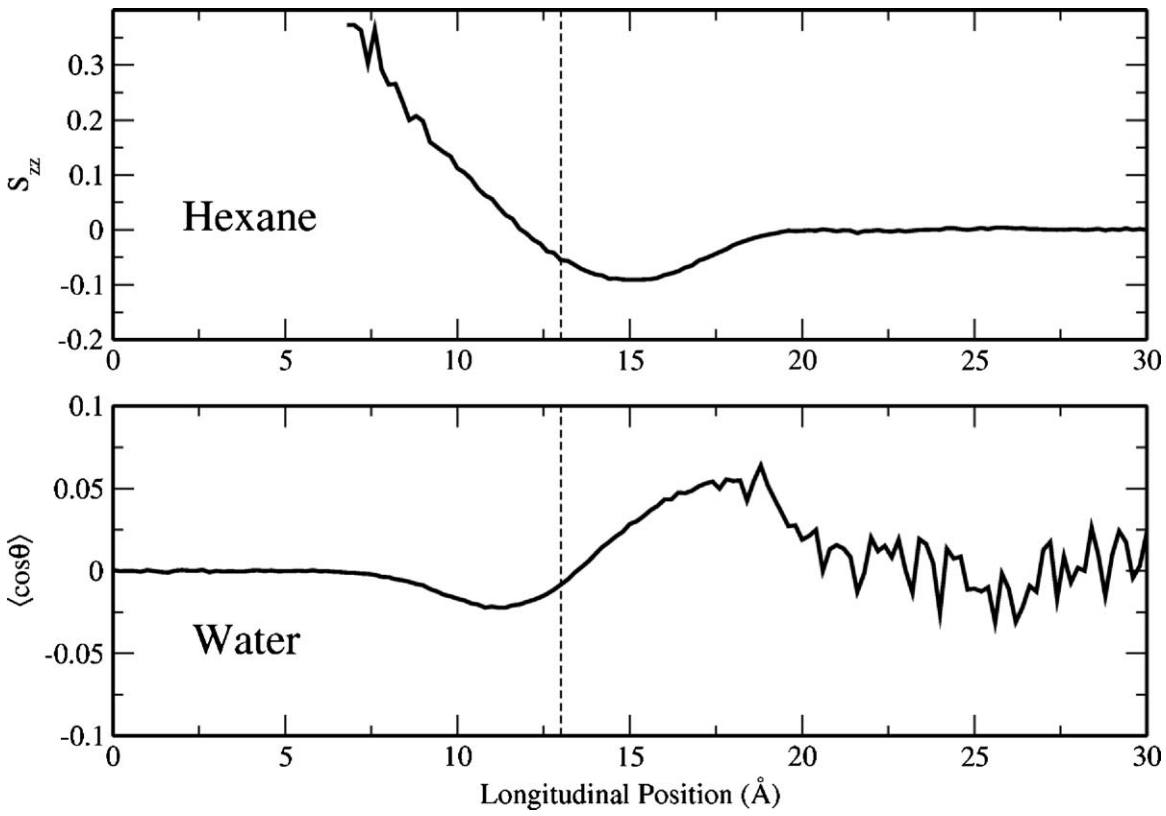

Fig. 3. Orientational profiles for the hexane and water as functions of longitudinal position relative to the center of mass of the system. S_{zz} is defined by Eq. (21) and θ is the angle between the normal of the interface and the water permanent dipole moment. The total system Gibbs dividing surface is indicated by the dashed vertical line.

into the aqueous phase, the hexane order parameter increases and ultimately becomes positive, indicating a transition to orientations favoring alignment along the interface normal, again as observed in earlier studies of decane–water interfaces. Interestingly, the behavior of hexane orientation moving through from hexane to water across the hexane–water interface is opposite that observed for transitioning from the pure bulk alkanes to the vapor [50].

3.2.2. Dipole moment profiles

A key characteristic of an interface consisting of two phases with vastly different dielectrics is the variation of molecular dipole moments from the bulk to the interfacial region. Previous studies of the hexane–water interface utilizing CHEQ force fields have shown that these models can account for this variation [44]. Fig. 4 shows the dipole moment profiles for hexane and water. As would be expected, the average water dipole moment monotonically drops

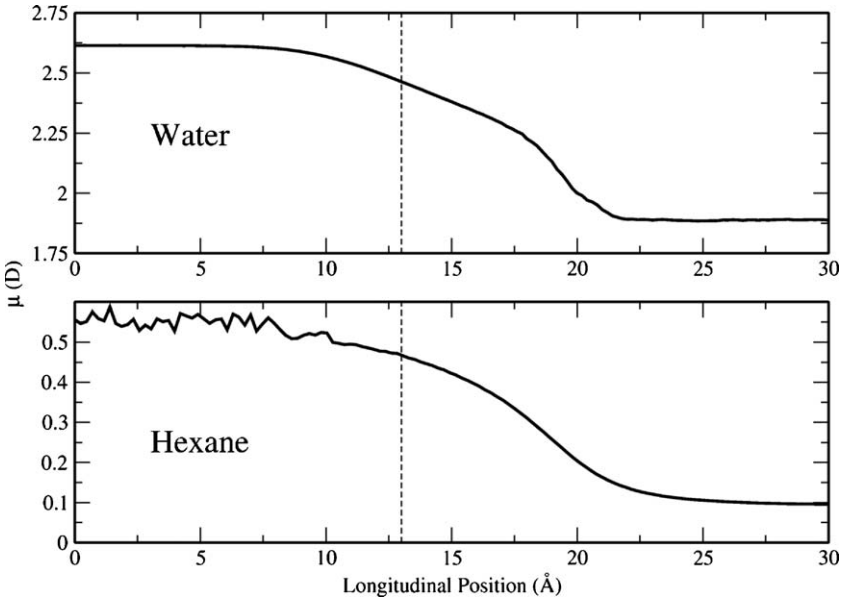

Fig. 4. Dipole moments of the hexane–water interfacial system as functions of longitudinal position relative to the center of mass of the system. The total system Gibbs dividing surface is indicated by the dashed vertical line.

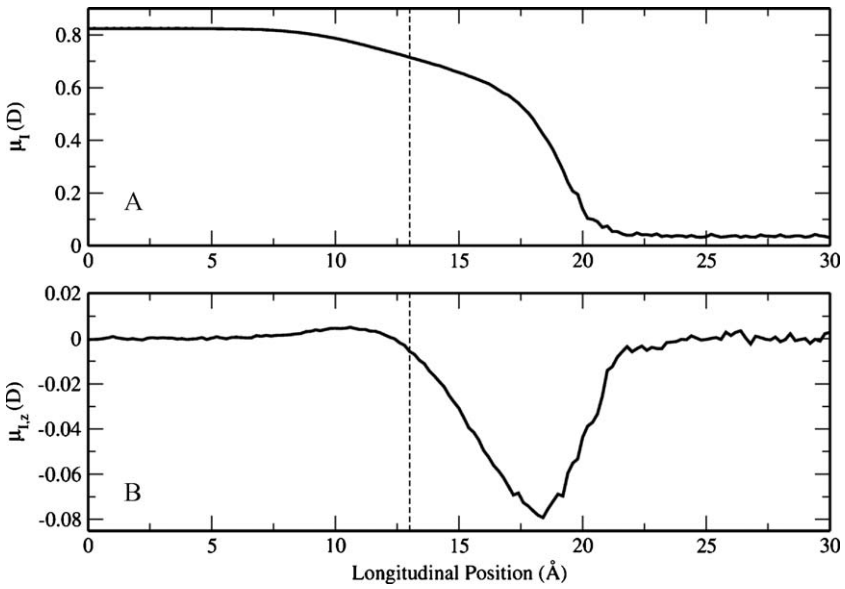

Fig. 5. (A) Average magnitude of the total induced dipole moment of water. (B) Average magnitude of the *z*-component of the induced dipole moment of water. Profiles are shown as functions of the longitudinal position relative to the center of mass of the system. The total system Gibbs dividing surface is indicated by the dashed vertical line.

from 2.61 D in bulk phase to 1.89 D, which is slightly above the gas-phase value of 1.85 D [45]. The hexane dipole moment exhibits a drastic increase in average dipole moment from 0.095 to 0.55 D as it crosses the interface. The quantitative accuracy of these measurements is difficult to assess due to the very small number of alkane molecules that enter the interface; however, a qualitative assessment shows that this result is a clear improvement over nonpolarizable models and has a less dramatic increase than in previous CHEQ models [44]. It is clear that polarizable force fields account for variations in molecular dipole moments, allowing for a more accurate representation of the dipolar nature of molecules traversing an interface of varying dielectric environments.

The average induced dipole moment, μ_I, of water has a profile (Fig. 5) similar in shape to the total dipole moment of water. The average induced dipole moment of water in bulk is 0.82 D and monotonically decreases to 0.035 D in bulk hexane, yielding similar results in both shape and magnitude to other water models [59–63]. We note that the difference between the magnitude of the total dipole moment vector of water and the magnitude of the fixed dipole moment vector is less than that of the induced dipole moment vector. This indicates that in an individual water molecule, the total dipole moment vector is often not aligned with the fixed dipole moment vector, meaning that the charge distribution within an individual water molecule is asymmetrical. This is a subtlety accounted for by the CHEQ formalism. Fig. 6 shows the average angle between the total dipole moment vector and the fixed dipole moment vector. In bulk the two vectors have an average angle of 6.6° and in the interface reach a maximum average angle of 10.4° while, in hexane the angle is less than 1°. We point out that the CHEQ water model we use does not possess the correct symmetric polarizability tensor since out of plane charge transfer to effect polarization in this direction is not incorporated. We acknowledge this deficiency in the water force field. With regard to water orientation, we suggest that an enhanced in-plane polarizability, introduced in this model to account for the lack of out-of-plane polarization, can lead to enhanced orientational structure in anisotropic environments such as interfaces. Though the structural behavior is not substantially different from current fixed-charge force fields, electrostatic properties associated with an interface will be affected. One such property would be interfacial electrostatic potentials, which may be enhanced due to enhanced structural ordering. For transfer of charged species across such interfaces, we acknowledge that certain care must be taken when interpreting results.

Fig. 5 shows the average magnitude of the *z*-component of the induced dipole $\mu_{I,z}$. The profile is similar in shape and magnitude to previous studies of the water–vapor interface using TIP4P-FQ [62]. A slight positive increase is observed at 12 Å. This increase is not seen in previous simulations of neat water at the liquid–vapor interface, but is seen when ions are present [62]. It cannot be determined if this increase is due to the polarizability of the hexane model or solely the presence of the hexane. A study utilizing fixed charge hexane models with TIP4P-FQ would further elucidate the cause of this feature (though such a study is outside the scope of this work).

3.2.3. Interfacial potential

The difference in electrostatic potential between the hexane phase and the water phase is an important property when

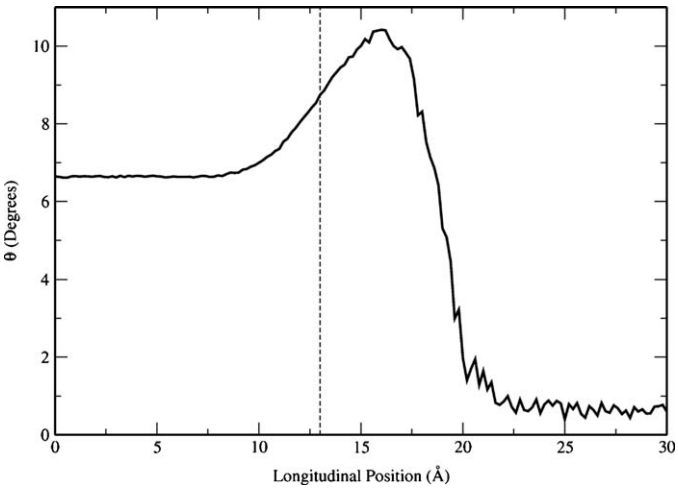

Fig. 6. Average angle between the fixed dipole moment and total dipole moment of water in the water–hexane interfacial system as a function of longitudinal position relative to the center of mass of the system. The total system Gibbs dividing surface is indicated by the dashed vertical line.

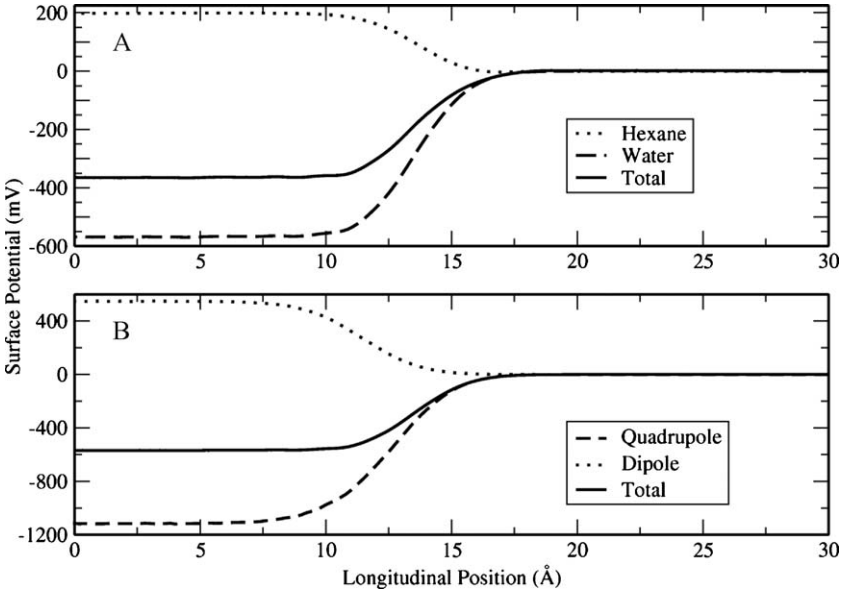

Fig. 7. (A) Interfacial potentials for the water–hexane system. Shown are the individual contributions from the hexane and the water as well as the total potential. (B) Quadrupole and dipole components of the water contribution to the interfacial potential of the water–hexane system.

determining whether a force field accurately models microscopic interfacial properties. Here we compute the interfacial potential from the charge density profile as generated from the z-dependent average charge [64]. The potential is then the solution of the Poisson equation:

$$\phi(z) - \phi(z_0) = \frac{-1}{\varepsilon_0} \int_{z_0}^{z} dz' \int_{z_0}^{z'} dz'' \rho^e(z'') \tag{22}$$

where ρ^e is the charge density and z_0 is a reference point in the hexane phase where the potential is taken to be zero. It is assumed that the electric field is constant in the plane parallel to the interface. Fig. 7A shows the interfacial potential across the hexane–water interface. Profiles of the water and hexane contributions are shown along with the total potential. The interfacial potential is calculated to be -364.7 ± 0.11, -567.9 ± 0.13, and 198.7 ± 0.01 mV for the total, water, and hexane contributions, respectively. The total potential is consistent with the reported experimental potentials across solvated lipid bilayers, which range from -400 to -600 mV [65–69]. However, as recently reported by Harder et al., care must be taken to compare the Galvani potential computed via simulation to the experimentally determined values based on free energetics of permeant ions [70]. Because the water has the greatest effect on the interfacial potential, a decomposition of the water interfacial potential was performed in order to determine the relative contributions arising from the water dipole and quadrupole moments. The potential due to the dipole moment was calculated via integration of the dipole moment density profile:

$$\Delta\Phi_M(z) = \frac{-1}{\varepsilon_0} \int_{z_0}^{\infty} dz\, P_z(z) \tag{23}$$

where P_z is the dipole moment density defined [71,72] as

$$P_z(z) = \left\langle \sum_m \delta(z - z_m) \left(\sum_i q_{im} z_{im} \right) \right\rangle. \tag{24}$$

Here m and i denote a molecule and an atomic site within that molecule, respectively. In these calculations the oxygen atom was taken as our molecule specific reference point z_m. The potential due to the quadrupole moment was calculated from the quadrupole moment density profile:

$$\Delta\Phi_Q(z) = \frac{-1}{\varepsilon_0} \left[Q_{zz}(z) - Q_{zz}^0 \right] \tag{25}$$

where Q_{zz}^0 is a reference value taken to be zero and situated far in the bulk hexane and the local quadrupole moment density profile Q_{zz} is defined [71,72] as

$$Q_{zz}(z) = \left\langle \sum_m \delta(z - z_m) \left(\sum_i q_{im} {z_{im}}^2 \right) \right\rangle. \tag{26}$$

Fig. 7B shows the potential due to the dipole moment, the quadrupole moment, and the total water potential. The calculated value of the water dipole and quadrupole are 547.5 ± 0.2 and -1116.8 ± 0.3 mV, respectively. The sum of these contributions agrees with the potential calculated for water using Eq. (22) to within less than 2 mV. This small difference is most likely a result of the exclusion of higher multipoles in the second method. Furthermore, the quadrupole contribution is the dominant component of the total water interfacial potential drop.

4. Phase transfer of small solutes

4.1. Potential of mean force

The potential of mean force of each species in the simulation was computed using umbrella sampling and the weighted histogram analysis method [43]. Profiles of the free energy (ΔG) characterizing the transfer of each solute across the water–hexane interface were obtained for water, hexane, methanol, ethanol, and 1-propanol. Fig. 8 shows the free energy profiles for water and hexane. The free energy cost of transferring a water molecule from water to bulk hexane is 4.48 ± 0.31 kcal/mol while transferring a hexane molecule from hexane to bulk water requires a free energy cost of 5.36 ± 0.22 kcal/mol. The lower cost of transferring water into hexane can account for the observation that a small, but noticeable number of water molecules fully penetrate the interface and enter the bulk hexane, remaining there for up to several nanoseconds. No penetration of hexane into bulk water is observed. The free energetic stabilization of water within the non-polar, dielectric hexane bulk region is similar to the observation of enhanced water

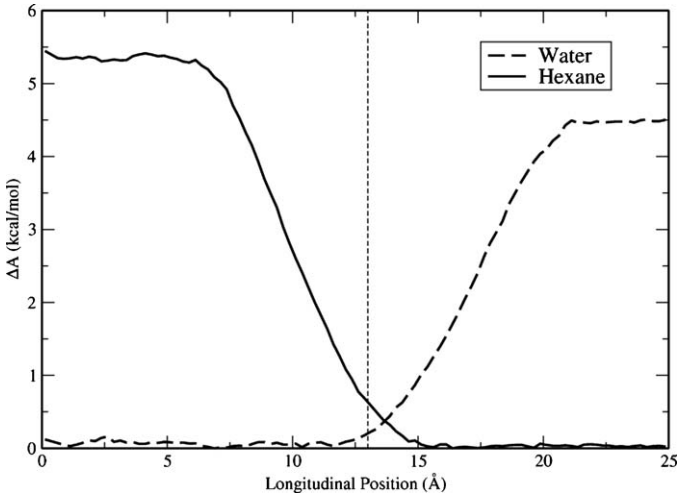

Fig. 8. Profiles of the free energy for transferring water and hexane across the interface are shown as functions of longitudinal position relative to the center of mass of the system. The total system Gibbs dividing surface is indicated by the dashed vertical line.

penetration within DMPC lipid bilayers are reported by Davis et al. [73]. The lowering of the water dipole in bulk hexane as shown in the top panel of Fig. 4 reduces the electrostatic penalty for water being desolvated relative to a fixed-charge representation. Effectively, the water dipole is modulated almost to its gas-phase value when in the bulk hexane region. This is a rather subtle but profound effect with implications for water-mediated transfer of polar solutes into lipid membranes.

The alcohol solutes all share similar free energy profiles characterized by a leveling off in the bulk water and bulk hexane phases and a minimum at the interface, with the minimum of the 1-propanol several angstroms closer to the hexane phase (Fig. 9). This general shape of the free energy profiles is expected for any amphiphilic molecule. Table 1 gives the free energy cost of transferring the alcohols from bulk water to the interface (ΔG_{w-i}), the interface to bulk hexane (ΔG_{i-h}), and bulk water to bulk hexane (ΔG_{w-h}). As expected, ΔG_{w-i} becomes more negative as the length of the carbon chain in the alcohol increases. The magnitude of ΔG_{w-i} values for methanol and ethanol are both higher than results

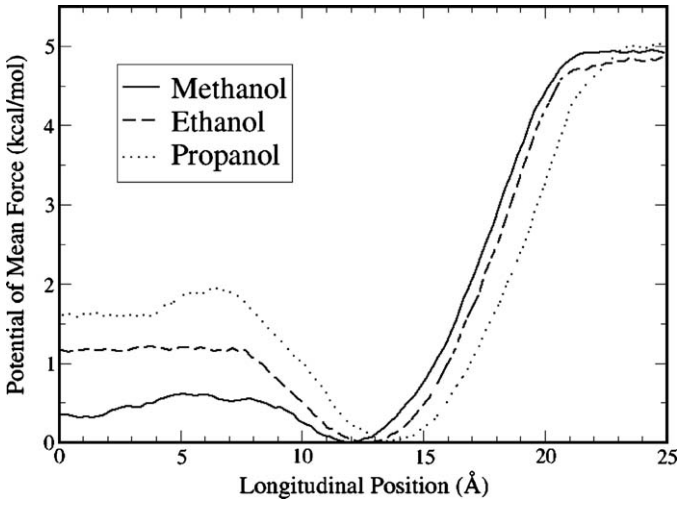

Fig. 9. Profiles of the free energy for transferring methanol, ethanol, and 1-propanol across the interface are shown as functions of longitudinal position relative to the center of mass of the system. Bulk water is centered at the origin; bulk hexane is centered at 25 Å.

Table 1
Free energies of transferring alcohols in the water–hexane interfacial system. Experimental data from Pohorille et al. [74]. No experimental data for 1-propanol was provided.

Molecule	ΔG_{w-i}	ΔG_{i-h}	ΔG_{w-h}	ΔG_{w-h} (experiment)
Methanol	−0.48 ± 0.13	4.93 ± 0.11	4.45 ± 0.18	3.59
Ethanol	−1.18 ± 0.08	4.83 ± 0.53	3.65 ± 0.49	2.73
1-Propanol	−1.61 ± 0.16	4.96 ± 0.21	3.35 ± 0.04	1.8[a]

[a] 1-Propanol value is an estimate based on linear interpolation from experimental data for methanol, ethanol, and 1-butanol [74].

reported by Pohorille et al. [74] by approximately 0.4–0.5 kcal/mol. This should be expected since allowing both the hexane and the carbon chain on the alcohol to polarize would allow for greater mixing than in a nonpolarizable model. The transfer of the alcohols from the interface to bulk hexane is essentially independent of the chain length. We calculate free energies of 4.8–4.96 kcal/mol for the transfer of alcohols from the interface to bulk hexane. This observation is qualitatively similar to the results of Pohorille et al. [74] that suggest an analogous value of 4.5 ± 0.3 kcal/mol.

4.2. Solvation free energies

To complement the investigation of the potential of mean force for the alcohol transfer across the water–hexane interface, we calculate the solvation free energies of each alcohol in pure water and pure hexane. We compute solvation free energies using the thermodynamic integration (TI) [75] approach:

$$\Delta G^{TI}_{\lambda_1+\lambda_2} = \Delta G^{TI}_{\lambda 1} + \Delta G^{TI}_{\lambda 2} = \int_0^1 d\lambda_1 \left\langle \frac{dH(\lambda_1)}{d\lambda_1} \right\rangle_{\lambda_2=0} + \int_0^1 d\lambda_2 \left\langle \frac{dH(\lambda_2)}{d\lambda_2} \right\rangle_{\lambda_1=1} \quad (27)$$

Here the free energy is computed along a two-step path that first decouples solvent-alcohol electrostatic interactions (λ_1) and then decouples solvent–alcohol Lennard–Jones terms (λ_2). The integrals of the system Hamiltonian were treated by summing the ensemble averages of discrete windows along each path. We decouple the electrostatic interactions via multiplication with a linear-scaling factor $(1-\lambda_1)$; a fully coupled state is represented by $\lambda_1 = 0$, whereas $\lambda_1 = 1$ is fully decoupled. Lennard–Jones decoupling was achieved using a modified "soft-core" interaction [76]:

$$U_{LJ}(\lambda_2) = \lambda_2 \left[\frac{A_f}{(r^2+\delta(1-\lambda_2))^6} - \frac{B_f}{(r^2+\delta(1-\lambda_2))^3} \right] + (1-\lambda_2) \left[\frac{A_i}{(r^2+\delta\lambda_2)^6} - \frac{B_i}{(r^2+\delta\lambda_2)^3} \right] \quad (28)$$

which allows for more thorough sampling near the fully decoupled end-point. A_i and B_i are the initial LJ parameters, A_f and B_f are the final LJ parameters (taken to be 0 for a fully decoupled state), and δ is soft-core shifting parameter. This shifting parameter was selected such that the decoupling path is essentially linear. We account for excluded long-range interactions beyond the simulation cutoff using the correction [40,77,78]:

$$\Delta G_{LRC} = \sum_i^{Solu.} \sum_j^{Solv.} 4\pi\rho \int_{r_{sw}}^{r_{cut}} U_{LJ,ij}(r)(1-S(r))r^2\,dr + 4\pi\rho \int_{r_{cut}}^{\infty} U_{LJ,ij}(r) r^2\,dr \quad (29)$$

in which ρ is the solvent density and $S(r)$ [79] is the switching function tapering the truncation of the Lennard–Jones potential

Table 2
Hydration free energies of alcohols in water and in hexane calculated using thermodynamic integration (TI); simulation values include long range corrections using Eq. (29). Experimental data from Pohorille et al. [74] except for (a) which is from Ref. [83]. Simulation values of alcohol hydration free energies in water are taken from Zhong et al. [37].

Molecule	ΔG_w	$\Delta G_{w,exp}$	ΔG_h	$\Delta G_{h,exp}$	ΔG_{w-h}	ΔG_{w-h} (exp)
Methanol	−5.97 ± 0.45	−4.94, −5.11[a]	−1.16 ± 0.02	−1.35	4.81 ± 0.45	3.59
Ethanol	−6.03 ± 0.45	−4.96, −5.01[a]	−1.98 ± 0.08	−2.23	4.05 ± 0.45	2.73
1-Propanol	−6.53 ± 0.47	−4.83[a]	−2.82 ± 0.05	−3.04	3.71 ± 0.47	1.8[b]
1-Butanol	−6.37 ± 0.36	−4.74, −4.72[a]	−3.56 ± 0.08	−3.87	2.81 ± 0.37	0.87

[b] 1-Propanol value is an estimate based on linear interpolation of experimental data for methanol, ethanol, and 1-butanol [74].

between r_{sw} and r_{cut}. The long-range correction is the taken as the sum over all LJ interactions between a solvent molecule and solute.

Results from the free energy of solvation calculations are shown in Table 2. The difference in solvation free energies of alcohols in water and hexane is consistently too favorable when compared to experimental values (i.e., the solute favor the aqueous phase). We note, however, that the ΔG_{w-h} values follow the anticipated trend in which the free energies of transferring larger alcohols from water to hexane become more favorable. The difference between the transfer free energies calculated using the PMF and TI approaches is appreciable, especially with larger alcohols. We also mention no long range corrections were considered for the PMF calculation, as was done for the TI calculations, which may also contribute to this discrepancy. Long-range corrections for alcohols in water and alcohols in hexane largely offset each other. Neglecting the long-range corrections in transfer free energies calculated using TI results increases the free energy by up to 0.1 kcal/mol for the alcohols studied. However, this is within the estimated error in this quantity.

We further assess the quality of the models used by comparing the solvation free energies in each solvent to experimental values. The magnitude of solvation free energy of the alcohols in hexane is consistently underpredicted by approximately 0.2–0.3 kcal/mol, while this quantity is overpredicted by over 1 kcal/mol in water. Though solvation free energies in both solvents exhibit discrepancy relative to experiment, the magnitudes of the two errors suggest that the overly favorable solvation of alcohols in water dominates the overly unfavorable transfer free energies (from water to hexane). The alcohol models utilized in this study were not explicitly parameterized to reproduce hydration free energies, although it is expected that including this property in the parameterization protocol will improve the quantitative agreement of the transfer free energies with experiment. Such work continues in our laboratory [37].

4.3. Dipole moment of alcohols

As previously discussed, the CHEQ model allows for the variation of the molecular dipole during the transport of solute across the interface of solutions of vastly different dielectric permittivity. Fig. 10 plots the average dipole moment of methanol, ethanol, and 1-propanol as a function of the z-position. In hexane the dipole moments for methanol, ethanol, and 1-propanol are 1.75, 1.73, and 1.63 D, respectively; each being slightly above the experimental gas phase values (1.70, 1.69, and 1.57 D) [45]. All three alcohols show a monotonic increase in their dipole moments through the interface. The dipole moments increase to 3.07, 2.69, and 2.79 D for methanol, ethanol, and 1-propanol, respectively. For methanol and ethanol the dipole moments in bulk water are within the expected range based upon previous studies of water–alcohol mixtures [80–82]. It is anticipated that the dipole moment of 1-propanol in bulk water would be less than the dipole moment of methanol and ethanol. However, we observe that 1-propanol has a dipole moment slightly larger than ethanol, indicating that the 1-propanol is likely slightly over-polarized despite the use of two charge normalization units.

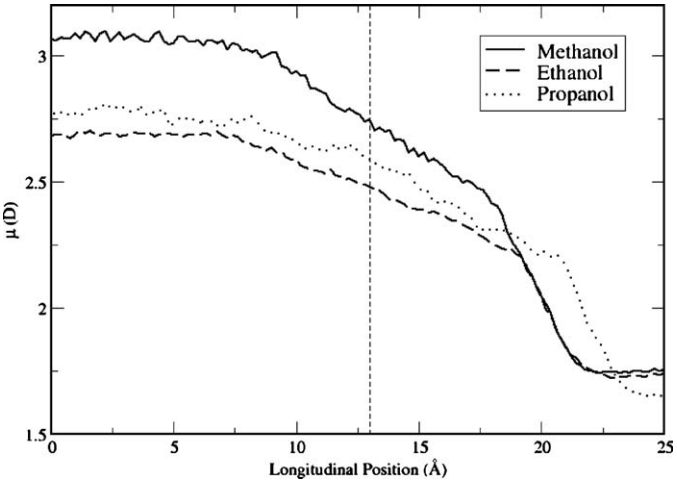

Fig. 10. Dipole moment profiles of methanol, ethanol and 1-propanol in the water–hexane system as functions of longitudinal position relative to the center of mass of the system. The total system Gibbs dividing surface is indicated by the dashed vertical line.

The fluctuations in the data arise from the fact that we sample dipole moments over 2 ns for a single alcohol molecule using the trajectories from the potential of mean force calculations at the specified windows.

5. Conclusions

We have presented results from molecular dynamics simulations of a water–hexane interfacial system using a charge equilibration force field. Bulk densities of hexane and water are well reproduced, as demonstrated by water and hexane bulk phase densities that agree with experiment to within 1 and 3%, respectively. We also observe the ability of the CHEQ model to account for the variation of electrostatic properties throughout the system. Our simulations show that in bulk hexane, a nonpolar environment, both water and hexane exhibit dipole moments slightly above their gas phase values. However, in bulk water, water and hexane both show an increase in dipole moment. This shift in dipole is an important aspect of such systems that is not captured by traditional fixed charge force fields. In the interfacial region, water reorients such that hydrogen bonding is maximized, while hexane orients parallel to the GDS. Interfacial potentials due to contributions of the water and hexane are calculated to be -567.9 ± 0.13 and 198.7 ± 0.01 mV, respectively, giving rise to a total potential in agreement with the range of values reported from previous simulations of similar systems. Finally, PMF profiles for the transfer of methanol, ethanol, and 1-propanol through the water–hexane interface were computed. Qualitatively, we observe the anticipated experimental trend in which transfer free energy of an alcohol from water to hexane decreases with increasing alcohol chain length. In all cases, the calculated transfer free energy from water to hexane is higher (more unfavorable) than experiment by 0.9–1.6 kcal/mol.

To verify these results, we employ thermodynamic integration approach to calculate the transfer free energy; the experimental trend is observed for the series methanol through 1-butanol. Results from both approaches agree with each other within the uncertainty of the calculation. Thermodynamic integration results are consistently higher than those from the PMF, which is partly due to the treatment of long-range corrections in the calculations of the former. In both cases, however, calculated free energies are too unfavorable. This is attributed to an overly favorable free energy of hydrating alcohols in water, although solvation free energy of alcohols in hexane matches experiment quite well.

Acknowledgments

The authors acknowledge generous support from NIH-sponsored COBRE at the University of Delaware, Department of Chemistry (5P20RR017716-07) and the University of Delaware's Howard Hughes Medical Institute Undergraduate Science Education Grant. B.A.B. acknowledges support through a University Graduate Fellows Award at the University of Delaware.

References

[1] A.J. Bard, L.R. Faulkner, Electrochemical Methods: Fundamentals and Applications, Wiley, New York, 1980.
[2] S. Haslam, et al., Surface second harmonic generation studies of the dodecane/water interface: the equilibrium and kinetic behavior of p-nitrophenol and tri-n-butyl phosphate, Phys. Chem. Chem. Phys. 2 (2000) 3235–3245.
[3] M.A. Wilson, A. Pohorille, Molecular dynamics of a water–lipid bilayer interface, J. Am. Chem. Soc. 116 (1994) 1490–1501.
[4] M.G. da Silveira, et al., Membrane fluidity adjustments in ethanol-stressed Oenococcus oeni cells, Appl. Environ. Microbiol. 69 (2003) 5826.
[5] H.V. Ly, D.E. Block, M.L. Longo, Interfacial tension effect on lipid bilayer rigidity, stability, and area/molecule: a micropipette aspiration approach, Langmuir 18 (2002) 8988.
[6] H.V. Ly, M.L. Longo, The influence of short-chain alcohols on interfacial tension, mechanical properties, area/molecule, and permeability of fluid lipid bilayers, Biophys. J. 87 (2004) 1013.
[7] W.R. Klemm, Biological, Water and its role in the effects of alcohol, Alcohol 15 (1998) 249.
[8] I.L. Carpenter, W.J. Hehre, A molecular dynamics study of the hexane–water interface, J. Phys. Chem. 94 (1990) 531–536.
[9] D. Michael, I. Benjamin, Solute orientational dynamics and surface roughness of water/hydrocarbon interfaces, J. Phys. Chem 99 (1995) 1530.
[10] J.P. Nicolas, N.R. de Souza, Molecular dynamics study of the n-hexane–water interface: towards a better understanding of the liquid–liquid interfacial broadening, J. Chem. Phys. 120 (5) (2004) 2464.
[11] J.L. Rivera, C. McCabe, P.T. Cummings, Molecular simulations of liquid-liquid interfacial properties: water–n-alkane and water–methanol–n-alkane systems, Phys. Rev. E 67 (2003) 011603.
[12] Y. Zhang, et al., J. Chem. Phys. 103 (1995) 10252.
[13] G. Lamoureux, A.D. Mackerell Jr., B. Roux, A simple polarizable model of water based on classical Drude oscillators, J. Chem. Phys. 119 (10) (2003) 5185–5197.
[14] G. Lamoureux, B. Roux, Modeling induced polarization with classical drude oscillators: theory and molecular dynamics simulation algorithm, J. Chem. Phys. 119 (6) (2003) 3025–3039.
[15] P. Ren, J.W. Ponder, Consistent treatment of inter- and intramolecular polarization in molecular mechanics calculations, J. Comput. Chem. 23 (16) (2002) 1497–1506.
[16] P. Ren, J.W. Ponder, Polarizable atomic multipole water model for molecular mechanics simulation, J. Phys. Chem. B 107 (2003) 5933–5947.
[17] S. Patel, C.L. Brooks III, Fluctuating charge force fields: recent developments and applications from small molecules to macromolecular biological systems, Mol. Simul. 32 (2006) 231–249.
[18] A.K. Rappe, W.A. Goddard III, Charge equilibration for molecular dynamics simulations, J. Phys. Chem. 95 (1991) 3358–3363.
[19] S.W. Rick, S.J. Stuart, B.J. Berne, Dynamical fluctuating charge force fields: application to liquid water, J. Chem. Phys. 101 (7) (1994) 6141–6156.
[20] J.E. Davis, G.L. Warren, S. Patel, A revised charge equilibration potential for liquid alkanes, J. Phys. Chem. B 112 (28) (2008) 8298–8310.
[21] S. Patel, C.L. Brooks III, A nonadditive methanol force field: bulk liquid and liquid–vapor interfacial properties via molecular dynamics simulations using a fluctuating charge model, J. Chem. Phys. (2005) 122.
[22] S. Patel, C.L. Brooks III, Structure, thermodynamics, and liquid–vapor equilibrium of ethanol from molecular dynamics simulations using nonadditive interactions, J. Chem. Phys. 123 (2005) 164502.
[23] S.W. Rick, Simulations of ice and liquid water over a range of temperatures using the fluctuating charge model, J. Chem. Phys. 114 (5) (2001) 2276.
[24] S.W. Rick, B.J. Berne, Dynamical fluctuating charge force fields: the aqueous solvation of amides, J. Am. Chem. Soc. 118 (1996) 672–679.
[25] S.W. Rick, S.J. Stuart, Potentials and algorithms for incorporating polarizability in computer simulations, in: K.B. Lipkowitz, D.B. Boyd (Eds.), Reviews in Computational Chemistry, John Wiley and Sons, Inc, 2002, p. 89.
[26] S.W. Rick, et al., Fluctuating charge force fields for aqueous solutions, J. Mol. Liquids 65–66 (1995) 31–40.
[27] S. Patel, A.D. MacKerell Jr., C.L. Brooks III, CHARMM fluctuating charge force field for proteins. II. Protein/solvent properties from molecular dynamics simulations using a non-additive electrostatic model, J. Comput. Chem. 25 (2004) 1504–1514.
[28] R.T. Sanderson, An interpretation fo bond lengths and a classification of bonds, Science 114 (1951) 670.
[29] R.T. Sanderson, Chemical Bonds and Bond Energy, 2nd ed., Academic, New York, 1976.
[30] R.F. Nalewajski, J. Korchowiec, Z. Zhou, Molecular hardness and softness parameters and their use in chemistry, Int. J. Quant. Chem.: Quant. Chem. Symp. 22 (1988) 349–366.
[31] R. Chelli, et al., Electrical response in chemical potential equalization schemes, J. Chem. Phys. 111 (18) (1999) 8569–8575.
[32] G.L. Warren, J.E. Davis, S. Patel, Origin and control of super-linear polarizability scaling in chemical potential equalizatioin methods, J. Chem. Phys. 128 (2008) 144110.
[33] R. Car, M. Parrinello, Unified approach for molecular dynamics and density-functional theory, Phys. Rev. Lett. 55 (1985) 2471.
[34] A.K. Al-Matar, D.A. Rockstraw, A generating equation for mixing rules and two new mixing rules for interatomic potential energy parameters, J. Comput. Chem. 25 (5) (2004) 660–668.
[35] J. Delhommelle, P. Millie, Inadequacy of the Lorentz–Berthelot combining rules for accurate predictions of equilibrium properties by molecular simulation, Mol. Phys. 99 (8) (2001) 619–625.
[36] C.M. Baker, et al., Accurate calculation of hydration free energies using pair-specific Lennard–Jones parameters in the CHARMM drude polarizable force field, J. Chem. Theory Comp. 6 (4) (2010) 1181–1198.
[37] Y. Zhong, S. Patel, Nonadditive empirical force fields for short-chain linear alcohols: methanol to butanol. Hydration free energies and Kirkwood–Buff analysis using charge equilibration models, J. Phys. Chem. B 114 (34) (2010) 11076–11092.
[38] B.R. Brooks, et al., CHARMM: a program for macromolecular energy, minimization, and dynamics calculations, J. Comput. Chem. 4 (1983) 187–217.
[39] J.P. Ryckaert, G. Ciccotti, H.J.C. Berendsen, Numerical-integration of cartesian equations of motion of a system with constraints—molecular dynamics of N-alkanes, J. Comput. Phys. 23 (1977) 327.
[40] M.P. Allen, D.J. Tildesley, Computer Simulation of Liquids, Clarendon Press, Oxford, 1987.
[41] G.J. Martyna, M.L. Klein, M. Tuckerman, Hose–Hoover chains: the canonical ensemble via continuous dynamics, J. Chem. Phys. 97 (4) (1992) 2635.
[42] T. Darden, D. York, L. Pederson, Particle mesh Ewald: an N log(N) method for Ewald sums in large systems, J. Chem. Phys. 98 (1993) 10089.
[43] S. Kumar, et al., The weighted histogram analysis method for free-energy calculations on biomolecules, J. Comput. Chem. 13 (1992) 1011–1021.
[44] S. Patel, C.L. Brooks III, Revisiting the hexane–water interface via molecular dynamics simulations using non-additive alkane–water potentials, J. Chem. Phys. 124 (2006) 204706.
[45] D.R. Lide, CRC Handbook of Chemistry and Physics, 84th ed., CRC Press LLC, New York, 2003.
[46] J. Chowdhary, B.M. Ladanyi, Water–hydrocarbon interfaces: effect of hydrocarbon branching on interfacial structure, J. Phys. Chem. B 110 (2006) 15442.
[47] S. Senapati, M.L. Berkowitz, Computer simulation study of the interface width of the liquid/liquid interface, Phys. Rev. Lett. 87 (17) (2001) 176101.
[48] P. Jungwirth, D.J. Tobias, Specific ion effects at the air/water interface, J. Chem. Rev. 106 (2006) 1259.
[49] L. Vrbka, et al., Propensity of soft ions for the air/water interface, Curr. Opin. Colloid Interface Sci. 9 (2004) 67.
[50] J.G. Harris, Liquid–vapor interfaces of alkane oligomers. Structure and thermodynamics from molecular dynamics simulations of chemically realistic models, J. Phys. Chem. 96 (1992) 5077–5086.
[51] J.G. Kirkwood, F.P. Buff, J. Chem. Phys. 17 (1949) 338.
[52] J.S. Rowlinson, B. Widom, Molecular Theory of Capillarity, Clarendon Press, Oxford, 1982.
[53] K.R. Wilson, et al., Surface relaxation in liquid water and methanol studied by X-ray absorption spectroscopy, J. Chem. Phys. 117 (16) (2002) 7738–7744.
[54] J. Cheng, M.R. Hoffman, A.J. Colussi, Anion fractionation and reactivity at air/water:methanol interfaces. Implication for the origin of Hofmeister effects, J. Phys. Chem. B 112 (24) (2008) 7157–7161.
[55] L.X. Dang, Ions at the liquid-vapor interface of methanol, J. Phys. Chem. A 108 (42) (2004) 904–9017.
[56] H. Stern, S.E. Feller, Calculation of the dielectric permitivity profile for a nonuniform system: application to a lipid bilayer simulation, J. Chem. Phys. 118 (2003) 3401.
[57] A.R.v. Buuren, S.-J. Marrink, H.J.C. Berendsen, A molecular dynamics study of the decane/water interface, J. Phys. Chem. 97 (1993) 9206–9209.
[58] B.A. Bauer, G.L. Warren, S. Patel, Incorporating phase-dependent polarizability in nonadditive electrostatic models for molecular dynamics simulations of the aqueous liquid–vapor interface, J. Chem. Theory Comput. 5 (2009) 359–373.

[59] G. Archontis, E. Leontidis, G. Andreou, Attraction of iodide ions by free water surface. Revealed by simulations with a polarizable force field based on drude oscillators, J. Phys. Chem. B 109 (2005) 17957.
[60] T. Ishiyama, A. Morita, Molecular dynamics study of gas–liquid aqueous sodium halide interfaces. I. Flexible and polarizable molecular modeling and interfacial properties, J. Phys. Chem. 111 (2007) 721.
[61] I.-F.W. Kuo, et al., Structure, dynamics, and thermodynamics of the aqueous liquid–vapor interface: a comprehensive particle-based simulations study, J. Phys. Chem. B 110 (2006) 3738–3746.
[62] G.L. Warren, S. Patel, Electrostatic properties of aqueous salt solution interfaces: a comparison of polarizable and nonpolarizable ion models, J. Phys. Chem. 112 (2008) 11679.
[63] C. Wick, et al., The effect of polarizability for understanding the molecular structure of aqueous interfaces, J. Chem. Theory Comput. 3 (2007) 2002.
[64] M.A. Wilson, A. Pohorille, L.R. Pratt, Surface potential of the water liquid–vapor interface, J. Chem. Phys. 88 (5) (1988) 3281–3285.
[65] R.F. Flewelling, W.L. Hubbel, The membrane dipole potential in a total membrane potential model, Biophys. J. 49 (1986) 541–552.
[66] K. Gawrisch, et al., Membrane dipole potentials, hydration forces, and the ordering of water at membrane surfaces, Biophys. J. 61 (5) (1992) 1213–1223.
[67] T.J. McIntosh, et al., Interbilayer interactions between sphingomyelin and sphingomyelin/cholesterol bilayers, Biochemistry 31 (1992) 2020–2024.
[68] V.L. Shapovalov, et al., Effect of gramicidin A on the dipole potential of phospholipid membranes, Biophys. J. 77 (1999) 299–305.
[69] S.A. Simon, T.J. McIntosh, Magnitude of the solvation pressure depends on dipole potential, PNAS 86 (1989) 9263–9267.
[70] E. Harder, B. Roux, On the origin of the electrostatic potential difference at a liquid–vacuum interface, J. Chem. Phys. 129 (2008) 234706.
[71] J.D. Jackson, Classical Electrodynamics, 3rd ed., Wiley, New York, 1998, p. 641.
[72] M.A. Wilson, A. Pohorille, Comment on "Study on the liquid–vapor interface of water. I. Simulation results of thermodynamic properties and orientational structure", J. Chem. Phys. 90 (1989) 5211.
[73] J.E. Davis, O. Rahaman, S. Patel, Molecular dynamics simulations of a DMPC bilayer using non-additive interaction models, Biophys. J. 96 (2009) 385–402.
[74] A. Pohorille, M.A. Wilson, C. Chipot, Interactions of alcohols and anesthetics with the water–hexane interface: a molecular dynamics study, Prog. Colloid Polym. Sci. 103 (1997) 29.
[75] T.P. Straatsma, J.A. McCammon, Multiconfiguration thermodynamic integration, J. Chem. Phys. 95 (1991) 1175.
[76] M. Zacharias, T.P. Straatsma, J.A. McCammon, Separation-shifted scaling, a new scaling method for Lennard–Jones interactions in thermodynamic integration, J. Chem. Phys. 100 (1994) 9025.
[77] M. Shirts, et al., Extremely precise free energy calculations of amino acid side chain analogs: comparison of common molecular mechanics force fields for proteins, J. Chem. Phys. 199 (11) (2003) 5740.
[78] J.T. Wescott, L.R. Fisher, S. Hanna, Use of thermodynamic integration to calculate the hydration free energies of n-alkanes, J. Chem. Phys. 116 (2002) 2361.
[79] G.L. Warren, S. Patel, Hydration free energies of monovalent ions in transferable intermolecular potential four point fluctuating charge water: an assessment of simulation methodology and force field performance and transferability, J. Chem. Phys. 127 (6) (2007) 17705614.
[80] T. Chang, L.X. Dang, Liquid–vapor interface of methanol–water mixtures: a molecular dynamics study, J. Phys. Chem. B 109 (2005) 5759.
[81] Y. Zhong, S. Patel, Electrostatic polarization effects and hydrophobic hydration in ethanol–water solutions from molecular dynamics simulations, J. Phys. Chem. B 113 (2009) 767.
[82] Y. Zhong, G.L. Warren, S. Patel, Thermodynamic and structural properties of methanol–water solutions using nonadditive interactions, J. Comput. Chem. 29 (2007) 1142.
[83] T. Ooi, et al., Accessible surface areas as a measure of the thermodynamic parameters of hydration of peptides, Proc. Natl. Acad. Sci. 84 (1987) 3086–3090.